

# Dark matter in galaxies: the dark matter particle mass is about 2 keV \*

H. J. de Vega <sup>(a)†</sup> and N. G. Sanchez <sup>(b)‡</sup>

<sup>(a)</sup> *LPTHE, Université Pierre et Marie Curie (Paris VI),  
Laboratoire Associé au CNRS UMR 7589, Tour 13, 4ème. et 5ème. étages,  
Boite 126, 4, Place Jussieu, 75252 Paris, Cedex 05, France.*

<sup>(b)</sup> *Observatoire de Paris, LERMA. Laboratoire Associé au CNRS UMR 8112.  
61, Avenue de l'Observatoire, 75014 Paris, France.*

(Dated: May 3, 2019)

Warm dark matter (WDM) means DM particles with mass  $m$  in the keV scale. For large scales, for structures beyond  $\sim 100$  kpc, WDM and CDM yield identical results which agree with observations. For intermediate scales, WDM gives the correct abundance of substructures. Inside galaxy cores, below  $\sim 100$  pc,  $N$ -body classical physics simulations are incorrect for WDM because at such scales quantum effects are important for WDM. Quantum calculations (Thomas-Fermi approach) provide galaxy cores, galaxy masses, velocity dispersions and density profiles in agreement with the observations. All evidences point to a dark matter particle mass around 2 keV. Baryons, which represent 16% of DM, are expected to give a correction to pure WDM results. The detection of the DM particle depends upon the particle physics model. Sterile neutrinos with keV scale mass (the main WDM candidate) can be detected in beta decay for Tritium and Rhenium and in the electron capture in Holmium. The sterile neutrino decay into X rays can be detected observing DM dominated galaxies and through the distortion of the black-body CMB spectrum. The effective number of neutrinos,  $N_{\text{eff}}$  measured by WMAP9 and Planck satellites is compatible with two Majorana sterile neutrinos with mass much smaller than the electron mass. One of them can be a WDM sterile neutrino.

So far, **not a single valid** objection arose against WDM.

## Contents

I. Introduction	1
II. Quantum physics in Galaxies	3
A. WDM Quantum pressure vs. gravitational pressure in compact galaxies	4
III. Quantum fermionic WDM gives the correct galaxy properties and galaxy profiles	5
IV. WDM gives the correct abundance of substructures	9
V. Detection of keV mass Sterile Neutrinos	9
VI. Sterile neutrinos and CMB fluctuations	11
VII. Future Perspectives and Sterile Neutrino Detection	12
References	12

## I. INTRODUCTION

81 % of the matter of the universe is **dark**. Dark matter (DM) is the dominant component of galaxies. DM interacts through gravity.

---

\* Based on Lectures given by H J de V at NuMass 2013, Milano-Bicocca, February 2013; at Cosmic Frontiers, SLAC, March 2013 and by H J de V and N G S at the Chalonge Torino Colloquium 2013, April 2013

†Electronic address: [devega@lpthe.jussieu.fr](mailto:devega@lpthe.jussieu.fr)

‡Electronic address: [Norma.Sanchez@obspm.fr](mailto:Norma.Sanchez@obspm.fr)

DM interactions other than gravitational have been **so far unobserved**, such possible couplings must be very weak: much weaker than weak interactions in particle physics. DM is outside the standard model of particle physics.

The main proposed candidates for DM are: Neutrinos (hot dark matter) back in the 1980's with particle mass  $m \sim 1$  eV already ruled out, Cold Dark Matter (CDM), weak interacting massive particles (WIMPs) in supersymmetric models with R-parity, with particle mass  $m \sim 10 - 1000$  GeV seriously disfavoured by galaxy observations, and finally Warm Dark Matter (WDM), mainly sterile neutrinos with particle mass  $m \sim 1$  keV.

DM particles decouple due to the universe expansion, their distribution function **freezes out** at decoupling. The characteristic length scale after decoupling is the **free streaming scale (or Jeans' scale)**. Following the DM evolution since ultrarelativistic decoupling by solving the linear Boltzmann-Vlasov equations yields (see for example [1]),

$$r_{Jeans} = 57.2 \text{ kpc} \frac{\text{keV}}{m} \left( \frac{100}{g_d} \right)^{\frac{1}{3}}, \quad (1.1)$$

where  $g_d$  equals the number of UR degrees of freedom at decoupling.

DM particles can **freely** propagate over distances of the order of the free streaming scale. Therefore, structures at scales smaller or of the order of  $r_{Jeans}$  are **erased** for a given value of  $m$ .

The observed size of the DM galaxy substructures is in the  $\sim 1 - 100$  kpc scale. Therefore, eq.(1.1) indicates that  $m$  should be in the keV scale. That is, Warm Dark Matter particles. This indication is confirmed by phase-space density observations [10] and relevant further evidence [3, 7, 11–14, 16–18].

For CDM particles with  $m \sim 100$  GeV we have  $r_{Jeans} \sim 0.1$  pc. Hence CDM structures keep forming till scales as small as the solar system. This result from the linear regime is confirmed as a **robust result** by  $N$ -body CDM simulations. However, it has **never been observed** in the sky.

Adding baryons to CDM does not cure this serious problem. There is **over abundance** of small structures in CDM and in CDM+baryons (also called the satellite problem).

CDM has **many serious** conflicts with observations as:

- Galaxies naturally grow through merging in CDM models. Observations show that galaxy mergers are **rare** ( $< 10\%$ ).
- Pure-disk galaxies (bulgeless) are observed whose formation through CDM is unexplained.
- CDM predicts **cusped** density profiles:  $\rho(r) \sim 1/r$  for small  $r$ . Observations show **cored** profiles:  $\rho(r)$  bounded for small  $r$ . Adding by hand strong enough feedback in the CDM from baryons can eliminate cusps but spoils the star formation rate.

Structures in the Universe as galaxies and cluster of galaxies form out of the small primordial quantum fluctuations originated by inflation just after the big-bang.

These linear small primordial fluctuations grow due to gravitational instabilities (Jeans) and then classicalize. Structures form through non-linear gravitational evolution. Hierarchical formation starts from small scales first.

$N$ -body CDM simulations **fail** to produce the observed structures for **small** scales less than some kpc.

Both  $N$ -body WDM and CDM simulations yield **identical and correct** structures for scales larger than some kpc.

At intermediate scales WDM give the **correct abundance** of substructures [14].

Inside galaxy cores, below  $\sim 100$  pc,  $N$ -body classical physics simulations are incorrect for WDM because quantum effects are important in WDM at these scales. WDM predicts correct structures for small scales (below kpc) when its **quantum** nature is taken into account [3].

The first ingredient in structure formation is the primordial power spectrum  $P(k)$ . We plot  $P(k)$  in fig. 1 for CDM and for several examples of WDM. CDM and WDM give identical results for the CMB fluctuations spectrum which correspond to large scales  $\gtrsim 1$  Mpc.

Warm dark matter has been the central subject of attention of recent Chalonge Colloquiums whose 'Highlights and Conclusions' are online [16].

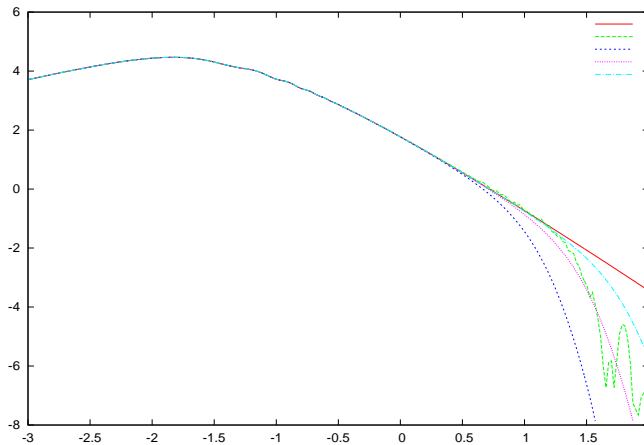


FIG. 1:  $\log_{10} P(k)$  vs.  $\log_{10}[k \text{ Mpc } h]$  for CDM in red, for 1 keV WDM in blue, 2 keV in violet and 4 keV WDM in light-blue DM particles decoupling in thermal equilibrium. 1 keV WDM sterile neutrinos decoupling out of thermal equilibrium are plotted in green. For WDM  $P(k)$  is cutted-off on small scales compared with CDM, that is  $r \lesssim 100 (\text{keV}/m)^{4/3} \text{ kpc}$ .

## II. QUANTUM PHYSICS IN GALAXIES

In order to determine whether a physical system has a classical or quantum nature one has to compare the average distance between particles with their de Broglie wavelength.

The de Broglie wavelength of DM particles in a galaxy can be expressed as

$$\lambda_{dB} = \frac{\hbar}{m v}, \quad (2.1)$$

where  $v$  is the velocity dispersion, while the average interparticle distance  $d$  can be estimated as

$$d = \left(\frac{m}{\rho_h}\right)^{\frac{1}{3}}, \quad (2.2)$$

where  $\rho_h$  is the average density in the galaxy core. We can measure the classical or quantum character of the system by considering the ratio

$$\mathcal{R} \equiv \frac{\lambda_{dB}}{d}$$

By using the phase-space density,

$$Q_h \equiv \frac{\rho_h}{\sigma^3}$$

and eqs.(2.1)-(2.2),  $\mathcal{R}$  can be expressed as [3]

$$\mathcal{R} = \hbar \left(\frac{Q_h}{m^4}\right)^{\frac{1}{3}}. \quad (2.3)$$

Notice that  $\mathcal{R}$  as well as  $Q_h$  are invariant under the expansion of the universe because the lengths  $\lambda_{dB}$  and  $d$  both scale with the expansion scale factor.  $\mathcal{R}$  and  $Q_h$  evolve by nonlinear gravitational relaxation.

Using now the observed values of  $Q_h$  from Table I yields  $\mathcal{R}$  in the range

$$2 \times 10^{-3} \left(\frac{\text{keV}}{m}\right)^{\frac{4}{3}} < \mathcal{R} < 1.4 \left(\frac{\text{keV}}{m}\right)^{\frac{4}{3}} \quad (2.4)$$

The larger value of  $\mathcal{R}$  is for ultracompact dwarfs while the smaller value of  $\mathcal{R}$  is for big spirals.

The ratio  $\mathcal{R}$  around unity clearly implies a macroscopic quantum object. Notice that  $\mathcal{R}$  expresses solely in terms of  $Q$  and hence  $(\hbar^3 Q/m^4)$  measures how quantum or classical is the system, here, the galaxy. Therefore, eq.(2.4) clearly shows **solely from observations** that compact dwarf galaxies are natural macroscopic quantum objects for WDM [3].

We see from eq.(2.4) that for CDM, that is for  $m \gtrsim \text{GeV}$ ,

$$\mathcal{R}_{CDM} \lesssim 10^{-8}$$

and therefore quantum effects are negligible in CDM.

### A. WDM Quantum pressure vs. gravitational pressure in compact galaxies

For an order-of-magnitude estimate, let us consider a halo of mass  $M$  and radius  $R$  of fermionic matter. Each fermion can be considered inside a cell of size  $\Delta x \sim 1/n^{1/3}$  and therefore has a momentum

$$p \sim \frac{\hbar}{\Delta x} \sim \hbar n^{1/3}.$$

The associated quantum pressure  $P_q$  (flux of the momentum) has the value

$$P_q = n \sigma p \sim \hbar \sigma n^{4/3} = \frac{\hbar^2}{m} n^{5/3}. \quad (2.5)$$

where  $v$  is the mean velocity given by

$$v = \frac{p}{m} = \frac{\hbar}{m} n^{1/3}.$$

The number density can be estimated as

$$n = \frac{M}{\frac{4}{3}\pi R^3 m},$$

and we use that  $p = m v$  to obtain from eq.(2.5) the quantum pressure

$$P_q = \frac{\hbar^2}{m R^5} \left( \frac{3 M}{4 \pi m} \right)^{5/3}. \quad (2.6)$$

On the other hand, as is well known, galaxy formation as all structure formation in the Universe is driven by gravitational physics. The system will be in dynamical equilibrium if this quantum pressure is balanced by the gravitational pressure

$$P_G = \text{gravitational force/area} = \frac{G M^2}{R^2} \times \frac{1}{4 \pi R^2} \quad (2.7)$$

Equating  $P_q = P_G$  from eqs.(2.7)-(2.6) yields the following expressions for the size  $R$  and the velocity  $v$  in terms of the mass  $M$  of the system and the mass  $m$  of the particles [3]:

$$R = \frac{3^{5/3}}{(4 \pi)^{2/3}} \frac{\hbar^2}{G m^{8/3} M^{1/3}} = 10.61 \dots \text{pc} \left( \frac{10^6 M_\odot}{M} \right)^{1/3} \left( \frac{\text{keV}}{m} \right)^{8/3}, \quad (2.8)$$

$$v = \left( \frac{4 \pi}{81} \right)^{1/3} \frac{G}{\hbar} m^{4/3} M^{2/3} = 11.62 \dots \frac{\text{km}}{\text{s}} \left( \frac{m}{\text{keV}} \right)^{4/3} \left( \frac{M}{10^6 M_\odot} \right)^{2/3}. \quad (2.9)$$

Notice that the values of  $M$ ,  $R$  and  $v$  are consistent with the observed values of dwarf galaxies. Namely, for  $M$  of the order  $10^6 M_\odot$  (which is a typical mass value for dwarf galaxies),  $R$  and  $v$  give the correct order of magnitude for the size and velocity dispersion of dwarf galaxies as displayed in Table I, for WDM particle mass in the keV scale.

These results back the idea that dwarf galaxies are supported by the fermionic *WDM quantum pressure* eq.(2.6) [3].

Galaxy	$r_h$ pc	$v$ $\frac{\text{km}}{\text{s}}$	$\frac{\hbar^{\frac{3}{2}} \sqrt{Q_h}}{(\text{keV})^2}$	$\rho(0)/\frac{M_\odot}{(\text{pc})^3}$	$\frac{M_h}{10^6 M_\odot}$
Willman 1	19	4	0.85	6.3	0.029
Segue 1	48	4	1.3	2.5	1.93
Leo IV	400	3.3	0.2	.19	200
Canis Venatici II	245	4.6	0.2	0.49	4.8
Coma-Berenices	123	4.6	0.42	2.09	0.14
Leo II	320	6.6	0.093	0.34	36.6
Leo T	170	7.8	0.12	0.79	12.9
Hercules	387	5.1	0.078	0.1	25.1
Carina	424	6.4	0.075	0.15	32.2
Ursa Major I	504	7.6	0.066	0.25	33.2
Draco	305	10.1	0.06	0.5	26.5
Leo I	518	9	0.048	0.22	96
Sculptor	480	9	0.05	0.25	78.8
Boötes I	362	9	0.058	0.38	43.2
Canis Venatici I	1220	7.6	0.037	0.08	344
Sextans	1290	7.1	0.021	0.02	116
Ursa Minor	750	11.5	0.028	0.16	193
Fornax	1730	10.7	0.016	0.053	1750
NGC 185	450	31	0.033	4.09	975
NGC 855	1063	58	0.01	2.64	8340
Small Spiral	5100	40.7	0.0018	0.029	6900
NGC 4478	1890	147	0.003	3.7	$6.55 \times 10^4$
Medium Spiral	$1.9 \times 10^4$	76.2	$3.7 \times 10^{-4}$	0.0076	$1.01 \times 10^5$
NGC 731	6160	163	$9.27 \times 10^{-4}$	0.47	$2.87 \times 10^5$
NGC 3853	5220	198	$8.8 \times 10^{-4}$	0.77	$2.87 \times 10^5$
NGC 499	7700	274	$5.9 \times 10^{-4}$	0.91	$1.09 \times 10^6$
Large Spiral	$5.9 \times 10^4$	125	$0.96 \times 10^{-4}$	$2.3 \times 10^{-3}$	$1. \times 10^6$

TABLE I: Observed values  $r_h$ , velocity dispersion  $v$ ,  $\sqrt{Q_h}$ ,  $\rho(0)$  and  $M_h$  covering from ultracompact galaxies to large spiral galaxies from refs.[4–9]. The phase space density is larger for smaller galaxies, both in mass and size. Notice that the phase space density is obtained from the stars velocity dispersion which is expected to be smaller than the DM velocity dispersion. Therefore, the reported  $Q_h$  are in fact upper bounds to the true values [8].

### III. QUANTUM FERMIONIC WDM GIVES THE CORRECT GALAXY PROPERTIES AND GALAXY PROFILES

We consider a single DM halo in the late stages of structure formation when DM particles composing it are non-relativistic and their phase-space distribution function  $f(t, \mathbf{r}, \mathbf{p})$  is relaxing to a time-independent form, at least for  $\mathbf{r}$  not too far from the halo center. In the Thomas-Fermi approach such a time-independent form is taken to be an energy distribution function  $f(E)$  of the conserved single-particle energy  $E = p^2/(2m) - \mu$ , where  $m$  is the mass of the DM particle and  $\mu$  is the chemical potential

$$\mu(\mathbf{r}) = \mu_0 - m\phi(\mathbf{r}) \quad (3.1)$$

with  $\phi(\mathbf{r})$  the gravitational potential and  $\mu_0$  some constant. We consider the spherical symmetric case.

Here, the Poisson equation for  $\phi(r)$  is a nonlinear and selfconsistent equation

$$\frac{d^2\mu}{dr^2} + \frac{2}{r} \frac{d\mu}{dr} = -4\pi G m \rho(r), \quad (3.2)$$

where the mass density  $\rho(r)$  is a function of  $\mu(r)$  and  $G$  is Newton's constant.  $\rho(r)$  is expressed here as a function

of  $\mu(r)$  through the standard integral of the DM phase-space distribution function over the momentum for Dirac fermions as

$$\rho(r) = \frac{m}{\pi^2 \hbar^3} \int_0^\infty dp p^2 f\left(\frac{p^2}{2m} - \mu(r)\right), \quad (3.3)$$

Another standard integral of the DM phase-space distribution function is the pressure

$$P(r) = \frac{1}{3\pi^2 m \hbar^3} \int_0^\infty dp p^4 f\left(\frac{p^2}{2m} - \mu(r)\right). \quad (3.4)$$

From  $\rho(r)$  and  $P(r)$  other quantities of interest, such as the velocity dispersion  $\sigma(r)$  and the phase-space density  $Q(r)$  can be determined as

$$\sigma^2(r) = \frac{P(r)}{\rho(r)}, \quad Q(r) = \frac{\rho(r)}{\sigma^3(r)}. \quad (3.5)$$

We see that  $\mu(r)$  fully characterizes the fermionic DM halo in this Thomas-Fermi framework. The chemical potential is monotonically decreasing in  $r$  since eq. (3.2) implies

$$\frac{d\mu}{dr} = -\frac{G m M(r)}{r^2}, \quad M(r) = 4\pi \int_0^r dr' r'^2 \rho(r'). \quad (3.6)$$

Moreover, the fermionic DM mass density  $\rho$  is bounded at the origin due to the Pauli principle [3], and therefore the proper boundary condition at the origin is

$$\frac{d\mu}{dr}(0) = 0. \quad (3.7)$$

Eqs.(3.2) and (3.3) provide an ordinary nonlinear differential equation that determines selfconsistently the chemical potential  $\mu(r)$  and constitutes the Thomas-Fermi semi-classical approach. We obtain a family of solutions parametrized by the value of  $\mu_0 \equiv \mu(0)$  [3].

In this semi-classical framework the stationary energy distribution function  $f(E)$  must be assigned beforehand. In a full-fledged treatment one would solve the cosmological DM evolution since decoupling till today, including the quantum dynamics in the evolution which become important in the non-linear stage and close enough to the origin.

We integrate the Thomas-Fermi nonlinear differential equations (3.2)-(3.3) from  $r = 0$  till the boundary  $r = R = R_{200} \sim R_{vir}$  defined as the radius where the mass density equals 200 times the mean DM density [3].

We define the core size  $r_h$  of the halo by analogy with the Burkert density profile as

$$\frac{\rho(r_h)}{\rho_0} = \frac{1}{4}, \quad r_h = l_0 \xi_h. \quad (3.8)$$

To explicitly solve eq. (3.2)-(3.3) we need to specify the distribution function  $\Psi(E/E_0)$ . But many important properties of the Thomas-Fermi semi-classical approximation do not depend on the detailed form of the distribution function  $\Psi(E/E_0)$ . Indeed, a generic feature of a physically sensible one-parameter form  $\Psi(E/E_0)$  is that it should describe degenerate fermions for  $E_0 \rightarrow 0$ . That is,  $\Psi(E/E_0)$  should behave as the step function  $\theta(-E)$  in such limit. In the opposite limit,  $\mu/E_0 \rightarrow -\infty$ ,  $\Psi(E/E_0)$  describes classical particles, namely a Boltzmann distribution. As an example of distribution function, we consider the Fermi-Dirac distribution

$$\Psi_{FD}(E/E_0) = \frac{1}{e^{E/E_0} + 1}. \quad (3.9)$$

We define the dimensionless chemical potential  $\nu(r)$  as

$$\nu(r) \equiv \mu(r)/E_0 \quad \text{and} \quad \nu_0 \equiv \mu(0)/E_0.$$

Large positive values of the chemical potential at the origin  $\nu_0 \gg 1$  correspond to the degenerate fermions limit which is the extreme quantum case, and oppositely,  $\nu_0 \ll -1$  gives the diluted regime which is the classical limit. In this classical regime the Thomas-Fermi equations (3.2)-(3.3) become exactly the equations for a self-gravitating Boltzmann gas.

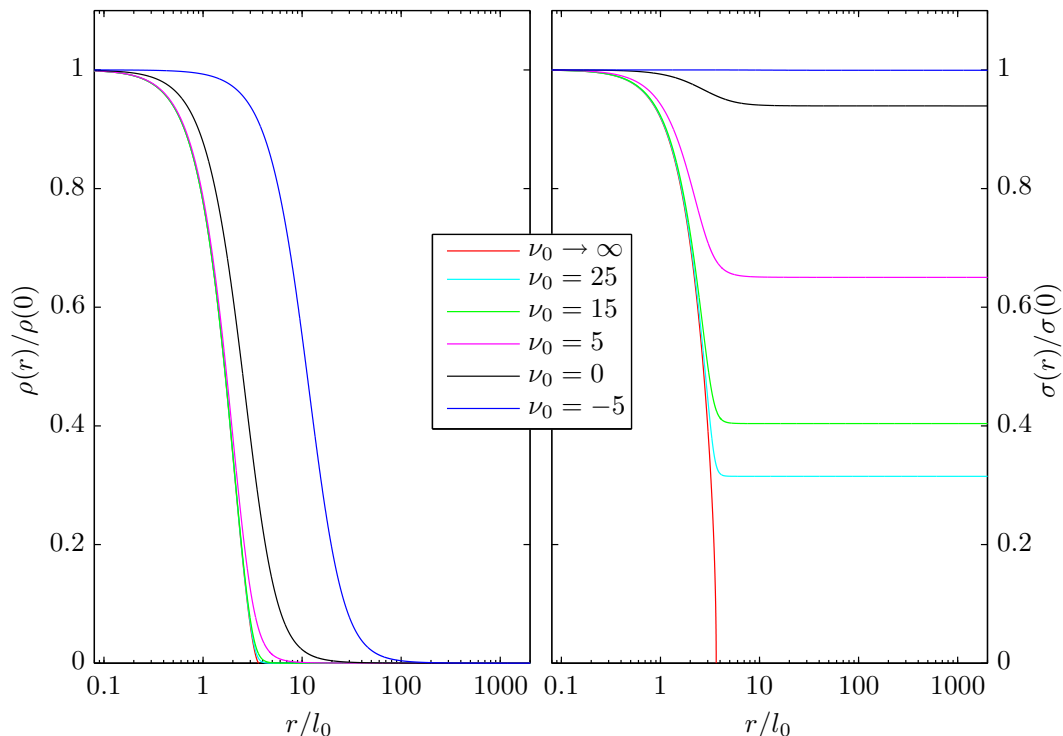


FIG. 2: Density and velocity profiles,  $\rho(r)/\rho_0$  and  $\sigma(r)/\sigma(0)$ , as functions of  $r/l_0$  for different values of the chemical potential at the origin  $\nu_0$  [3]. Large positive values of  $\nu_0$  correspond to compact galaxies, negative values of  $\nu_0$  correspond to the classical regime describing spiral and elliptical galaxies. All density profiles are cored. The sizes of the cores  $r_h$  defined by eq.(3.8) are in agreement with the observations, from the compact galaxies where  $r_h \sim 35$  pc till the spiral and elliptical galaxies where  $r_h \sim .2 - 60$  kpc. The larger and positive is  $\nu_0$ , the smaller is the core. The minimal one arises in the degenerate case  $\nu_0 \rightarrow +\infty$  (compact dwarf galaxies).

We display in fig. 2 the density and velocity profiles [3]. Namely, we plot  $\rho(r)/\rho_0$  and  $\sigma(r)/\sigma(0)$  as functions of  $r/R$  for  $\nu_0 \equiv \nu(0) = -5, 0, 5, 15, 25$  and for the degenerate fermion limit  $\nu_0 \rightarrow +\infty$ . The obtained fermion profiles are always cored. The sizes of the cores  $r_h$  defined by eq.(3.8) are in agreement with the observations, from the compact galaxies where  $r_h \sim 35$  pc till the spiral and elliptical galaxies where  $r_h \sim 0.2 - 60$  kpc. The larger and positive is  $\nu_0$ , the smaller is the core. The minimal core size arises in the degenerate case  $\nu_0 \rightarrow +\infty$  (compact dwarf galaxies).

In the left panel of fig. 3 we plot the dimensionless quantity [3]

$$\frac{\hbar^3}{(\text{keV})^4} Q(0). \quad (3.10)$$

In the right panel of fig. 3, we plot instead the dimensionless product

$$\frac{M_h}{M_\odot} \sqrt{\frac{1}{\rho_0} \frac{M_\odot}{\text{pc}^3}}, \quad (3.11)$$

where  $M_h$  is the halo mass, namely the galaxy mass inside the core radius  $r_h$  defined by eq.(3.8). In both cases we consider the two values  $m = 1$  and  $2$  keV and we put in the abscissa the product

$$r_h \left( \frac{\text{pc}^3}{M_\odot} \rho_0 \right)^{\frac{1}{6}} \quad \text{in parsecs,} \quad (3.12)$$

where  $r_h$  is the core radius. The phase-space density  $Q(0)$  and the galaxy mass  $M_h$  are obtained by solving the Thomas-Fermi eqs.(3.2)-(3.3). We have also superimposed the observed values  $\hbar^3 Q_h / (\text{keV})^4$  and  $M_h \sqrt{M_\odot / [\rho_0 \text{ pc}^3]}$  ( $m/\text{keV}$ )<sup>4</sup> from Table I. Notice that the observed values  $Q_h$  from the stars' velocity dispersion are in fact upper bounds for the

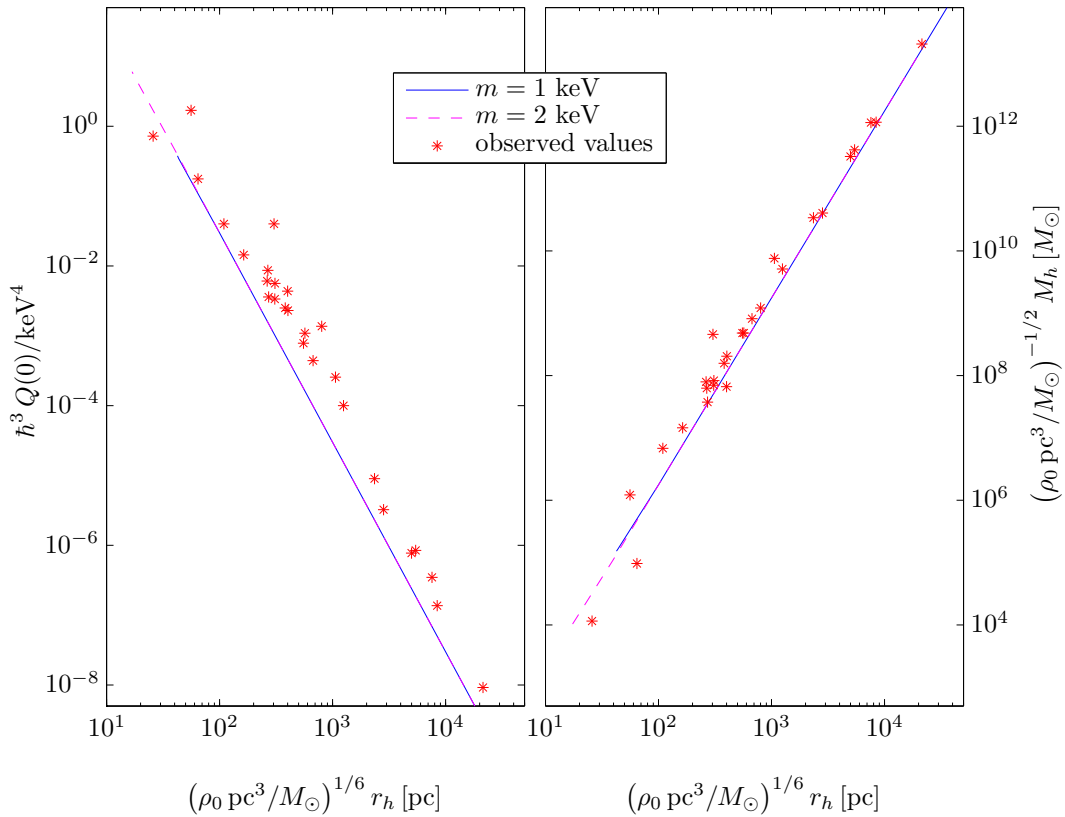


FIG. 3: In the left panel we display the galaxy phase-space density  $\hbar^3 Q(0)/(\text{keV})^4$  obtained from the numerical resolution of the Thomas-Fermi eqs. (3.2)-(3.3) for WDM fermions of mass  $m = 1$  and  $2$  keV versus the ordinary logarithm of the product  $\log_{10}\{r_h [\text{pc}^3 \rho_0/M_\odot]^{1/6}\}$  in parsecs [3]. The red stars  $*$  are the observed values of  $\hbar^3 Q(0)/(\text{keV})^4$  from Table I. Notice that the observed values  $Q_h$  from the stars' velocity dispersion are in fact upper bounds for the DM  $Q_h$  and therefore the theoretical curve is slightly below them. In the right panel we display the galaxy mass  $(M/M_\odot)\sqrt{M_\odot/[\rho_0 \text{ pc}^3]}$  obtained from the numerical resolution of the Thomas-Fermi eqs.(3.2)-(3.3) for WDM fermions of mass  $m = 1$  and  $2$  keV versus the product  $r_h [\text{pc}^3 \rho_0/M_\odot]^{1/6}$  in parsecs [3]. The red stars  $*$  are the observed values of  $(M/M_\odot)\sqrt{M_\odot/[\rho_0 \text{ pc}^3]}$  from Table I. Notice that the error bars of the observational data are not reported here but they are at least about  $10 - 20\%$ .

DM  $Q_h$ . This may explain why the theoretical Thomas-Fermi curves in the left panel of fig. 3 appear slightly below the observational data. Notice also that the error bars of the observational data are not reported here but they are at least about  $10 - 20\%$ .

The phase space density decreases from its maximum value for the compact dwarf galaxies corresponding to the limit of degenerate fermions till its smallest value for large galaxies, spirals and ellipticals, corresponding to the classical dilute regime. On the contrary, the halo radius  $r_h$  and the halo mass  $M_h$  monotonically increase from the quantum (small and compact galaxies) to the classical regime (large and dilute galaxies).

Thus, the whole range of values of the chemical potential at the origin  $\nu_0$  from the extreme quantum (degenerate) limit  $\nu_0 \gg 1$  to the classical (Boltzmann) dilute regime  $\nu_0 \ll -1$  yield all masses, sizes, phase space densities and velocities of galaxies from the ultra compact dwarfs till the larger spirals and elliptical in agreement with the observations (see Table I).

From figs. 3 we can extract important information on the fermion particle WDM mass.

We see from the left panel fig. 3 that decreasing the DM particle mass  $m$  moves the theoretical curves  $\hbar^3 Q(0)/(\text{keV})^4$  towards smaller  $Q(0)$  values and larger galaxy sizes, one over each other. In the right panel of fig. 3 we see that decreasing the DM particle mass  $m$  displaces the theoretical curves  $(M_h/M_\odot)\sqrt{M_\odot/[\rho_0 \text{ pc}^3]}$  towards larger galaxy masses and sizes, one over each other.

The small galaxy endpoint of the curves in figs. 3 corresponds to the degenerate fermion limit  $\nu_0 \rightarrow +\infty$  and its value depends on the WDM particle value  $m$ . For increasing  $m$ , the small galaxy endpoint moves towards smaller sizes while for decreasing  $m$ , it moves towards larger sizes.



We see from figs. 3 that decreasing the particle mass beyond a given value, namely for particle masses  $m \lesssim 1$  keV, the theoretical curves do not reach the more compact galaxy data. Therefore,  $m \lesssim 1$  keV is ruled out as WDM particle mass.

For growing  $m \gtrsim$  keV the left part of the theoretical curves corresponding to the lower galaxy masses and sizes, will not have observed galaxy counterpart. Namely, increasing  $m \gg$  keV would show an overabundance of small galaxies (small scale structures) which do not have counterpart in the data. This is a further indication that the WDM particle mass is approximately around 2 keV in agreement with earlier estimations [7, 10].

In addition, the galaxy velocity dispersions turn to be fully consistent with the galaxy observations in Table I [3].

To conclude, the galaxy magnitudes: halo radius, galaxy masses and velocity dispersion obtained from the Thomas-Fermi quantum treatment for WDM fermion masses in the keV scale are fully consistent with all the observations for all types of galaxies (see Table I). Namely, fermionic WDM treated quantum mechanically (as it must be) is able to reproduce the observed sizes of the DM cores of galaxies [3]. These results strenght the discussion in sec. II A that compact galaxies are supported against gravity by the fermionic WDM quantum pressure.

It is highly remarkably that in the context of fermionic WDM, the simple stationary quantum description provided by the Thomas-Fermi approach is able to reproduce such broad variety of galaxies.

Baryons have not yet included in the present study. This is fully justified for dwarf compact galaxies which are composed today 99.99% of DM. In large galaxies the baryon fraction can reach values up to 1 - 3 %. Fermionic WDM by itself produces galaxies and structures in agreement with observations for all types of galaxies, masses and sizes. Therefore, the effect of including baryons is expected to be a correction to these pure WDM results, consistent with the fact that dark matter is in average six times more abundant than baryons.

#### IV. WDM GIVES THE CORRECT ABUNDANCE OF SUBSTRUCTURES

It is known since some time through  $N$ -body simulations that WDM alleviates the CDM satellite problem [11, 12] and the CDM voids problem [13].

WDM subhalos turns to be less concentrated than CDM subhalos. WDM subhalos have the right concentration to host the bright Milky Way satellites [12].

The ALFALFA survey has measured the velocity widths in galaxies from the 21cm HI line. This is a test for substructure formation. The confrontation of the ALFALFA survey with the substructures from  $N$ -body simulations clearly favours WDM over CDM [14]. A particle mass around  $\sim 2$  keV is favoured by the ALFALFA survey.

In summary, WDM produces the correct substructure abundance at zero redshift.

Data on galaxy substructure for redshift  $z \lesssim 10$  becomes now available.

In ref. [17] the evolution of the observed AGN luminosity function for  $3 < z < 6$  is contrasted with the WDM and CDM simulations. WDM is clearly favoured over CDM by the observational data.

In ref. [18] the number of observed structures vs. the star formation rate for  $z = 5, 6, 7$  and  $8$  is contrasted with the results from WDM and CDM simulations. Again, WDM turns to be clearly favoured by the observations over CDM.

At intermediate scales where WDM and CDM give non-identical results and quantum effects are negligible,  $N$ -body classical simulations are reliable. Contrasting such  $N$ -body classical simulations results with astronomical observations at zero and non-zero redshifts **clearly favours** WDM over CDM.

For larger scales  $\gtrsim 100$  kpc, CDM and WDM  $N$ -body classical simulations are reliable and give identical results in good agreement with astronomical and cosmological observations.

#### V. DETECTION OF KEV MASS STERILE NEUTRINOS

Sterile neutrinos  $\nu_s$  are mainly formed by right-handed neutrinos  $\nu_R$  plus a small amount of left-handed neutrinos  $\nu_L$ . Conversely, active neutrinos  $\nu_a$  are formed by  $\nu_L$  plus a small amount of  $\nu_R$ :

$$\nu_s \simeq \nu_R + \theta \nu_L \quad , \quad \nu_a = \nu_L + \theta \nu_R .$$

Sterile neutrinos were named by Bruno Pontecorvo in 1968. They are singlets under all symmetries of the Standard Model of particle physics. Sterile neutrinos do not interact through weak, electro-magnetic or strong interactions.

WDM  $\nu_s$  are typically produced in the early universe from active neutrinos through mixing, namely, through a bilinear term  $\theta \nu_s \nu_a$  in the Lagrangian.

The appropriate value of the mixing angle  $\theta$  to produce enough sterile neutrinos  $\nu_s$  accounting for the observed total DM depends on the particle physics model and is typically very small:

$$\theta \sim 10^{-3} - 10^{-4} .$$

The smallness of  $\theta$  makes sterile neutrinos difficult to detect in experiments.

Sterile neutrinos can be detected in beta decay and in electron capture (EC) processes when a  $\nu_s$  with mass in the keV scale is produced **instead** of an active  $\nu_a$ :

$${}^3H_1 \implies {}^3He_2 + e^- + \bar{\nu}_e \quad , \quad {}^{187}Re \implies {}^{187}Os + e^- + \bar{\nu}_e .$$

In beta decays the electron spectrum is slightly modified at energies around the  $\nu_s$  mass ( $\sim$  keV) when a  $\bar{\nu}_s$  is produced instead of a  $\bar{\nu}_e$  in the decay products. Such event can be inferred observing the electron energy spectrum. A 'kink' should then appear around the energy of the  $\nu_s$  mass.

In electron capture processes like:

$${}^{163}Ho + e^- \implies {}^{163}Dy^* + \nu_e$$

when a  $\nu_s$  with mass in the keV scale is produced **instead** of an active  $\nu_e$ , the observed nonradiative de-excitation of the  $Dy^*$  is different to the case where an active  $\nu_e$  shows up.

The available energies for these beta decays and EC are

$$Q({}^{187}Re) = 2.47 \text{ keV} \quad , \quad Q({}^3H_1) = 18.6 \text{ keV} \quad , \quad Q({}^{163}Ho) \simeq 2.5 \text{ keV} . \quad (5.1)$$

In order to produce a sterile neutrino with mass  $m$ ,  $Q$  must be larger than  $m$ . However, in order to distinguish the sterile neutrino  $\nu_s$  from a practically massless active neutrino  $\nu_a$ ,  $Q$  must be as small as possible. This motivates the choice of the nuclei with the lowest known  $Q$  in eq.(5.1).

For a theoretical analysis of  $\nu_s$  detection in Rhenium and Tritium beta decay see ref.[19] and references therein.

Present experiments searching the small active neutrino mass also look for sterile neutrinos in the keV scale:

- MARE (Milan, Italy), Rhenium 187 beta decay and Holmium 163 electron capture [24].
- KATRIN (Karlsruhe, Germany), Tritium beta decay [25].
- ECHo (Heidelberg, Germany), Holmium 163 EC [26].
- Project 8 (Seattle, USA), Tritium beta decay [27].

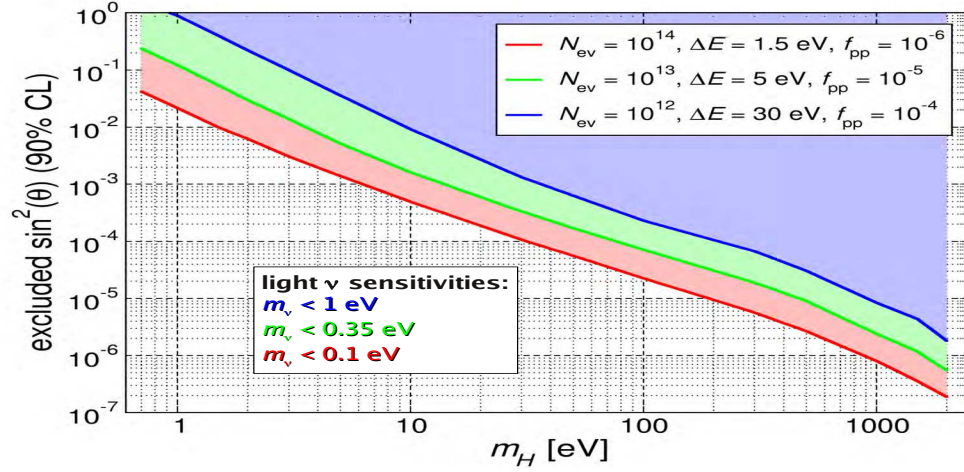
The more popular sterile neutrino models nowadays are:

- The Dodelson-Widrow (DW) model (1994): sterile neutrinos are produced by non-resonant mixing from active neutrinos.
- The Shi-Fuller model (SF) (1998): sterile neutrinos are produced by resonant mixing from active neutrinos.
- $\nu$ MSM model (2005): sterile neutrinos are produced by a Yukawa coupling from the decay of a heavy real scalar field  $\chi$ .
- Models based on: Froggatt-Nielsen mechanism, flavor symmetries,  $Q_6$ , split see-saw, extended see-saw, inverse see-saw, loop mass. Furthermore: scotogenic, LR symmetric, etc. See for a recent review [20].

WDM particles decoupling ultrarelativistically in the first three WDM particle models behave just as if their masses were different [2]. The masses of WDM particles in the first three models which give the same primordial power spectrum can be related according to the formula [2] (FD = thermal fermions):

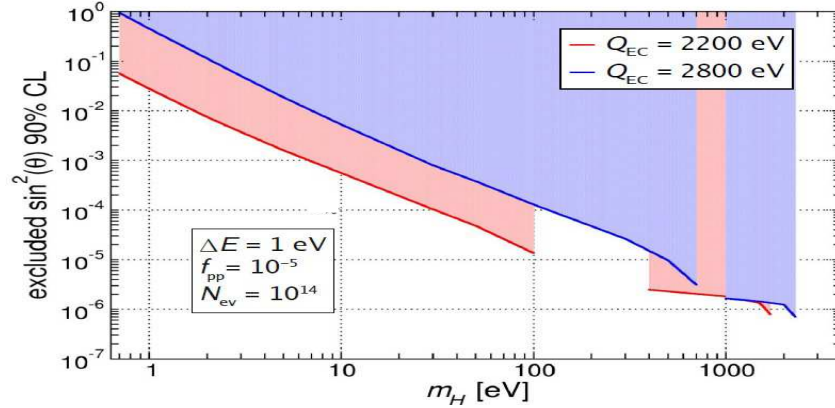
$$\frac{m_{DW}}{\text{keV}} \simeq 2.85 \left( \frac{m_{FD}}{\text{keV}} \right)^{\frac{4}{3}} \quad , \quad m_{SF} \simeq 2.55 m_{FD} \quad , \quad m_{\nu\text{MSM}} \simeq 1.9 m_{FD} .$$

**MARE sensitivity to heavy neutrinos:  $^{187}\text{Re}$  option**



A. Nucciotti, Meudon Workshop 2011, 8-10 JUNE 2011 36

**MARE sensitivity to heavy neutrinos: Ho option 2**



Meudon Workshop 2012, 6-8 June 2012

E. Ferri

32

For the primordial power spectrum, there is a degeneracy between these three models.

Sterile neutrinos  $\nu_s$  decay into active neutrinos  $\nu_a$  plus X-rays with an energy  $m/2$  [21]. The lifetime of  $\nu_s$  is about  $\sim 10^{11} \times$  age of the universe. The value of the lifetime depends on the particle physics neutrino model.

These X-rays may be seen in the sky looking to galaxies [22]. See [23] for a recent review.

Some future observations of X-rays from galaxy halos:

- DM bridge between M81 and M82  $\sim 50$  kpc. Overlap of DM halos. Satellite projects: Xenia (NASA) [28].
- CMB: WDM decay distorts the blackbody CMB spectrum. The projected PIXIE satellite mission can measure WDM sterile neutrino mass by measuring this distortion [29].

Active neutrinos are very abundant in supernovae explosions and in these explosions sterile neutrinos are produced too. Hence, bounds on the presence of sterile neutrinos can be obtained contrasting to supernovae observations. The results from supernovae do not constrain  $\theta$  provide  $1 < m < 10$  keV [30].

**VI. STERILE NEUTRINOS AND CMB FLUCTUATIONS**

CMB fluctuations data provide the effective number of neutrinos,  $N_{\text{eff}}$ . This effective number  $N_{\text{eff}}$  is related in a subtle way to the real number of active neutrinos (three) plus the number of sterile neutrinos with masses much smaller than the electron mass  $m_e$  [31].

As shown in ref. [32] (see fig. 8 in pag. 13 of ref. [32]) two Majorana sterile neutrinos with mass  $m \ll m_e$  are compatible with the Planck result:  $N_{\text{eff}} = 3.5 \pm 0.5$  (95%; Planck+WP+highL+H<sub>0</sub>+BAO) [33].

Therefore, Planck results are **compatible** with one Majorana sterile neutrino with an eV mass and one Majorana sterile neutrino with a keV mass. Indeed, other combinations of steriles are compatible with solely the value of  $N_{\text{eff}}$  [32]. All these analysis are within the standard cosmological model.

## VII. FUTURE PERSPECTIVES AND STERILE NEUTRINO DETECTION

WDM particle models must explain the baryon asymmetry of the universe. This is a strong constraint on sterile neutrino models which must be worked out for each model.

Combining particle, cosmological and galaxy results for sterile neutrinos at different mass scales [3, 10, 34–36], an appealing **mass** neutrino hierarchy appears:

- Active neutrino:  $\sim$  mili eV
- Light sterile neutrino:  $\sim$  eV
- Dark Matter sterile neutrino:  $\sim$  keV
- Unstable sterile neutrino:  $\sim$  MeV....

This scheme may represent the future extension of the standard model of particle physics.

In order to falsify WDM, comprehensive theoretical calculations showing substructures, galaxy formation and evolution including the quantum WDM effects in the dynamical evolution are needed to contrast with the astronomical observations.

In such WDM theoretical calculations the quantum pressure must be necessarily included. These calculations should be performed matching the semiclassical Hartree-Fock (Thomas-Fermi) dynamics in regions where the dimensionless phase-space density  $\hbar^3 Q/m^4 \gtrsim 0.1$  with the classical evolution in regions where  $\hbar^3 Q/m^4 \ll 1$ . These are certainly not easy numerical calculations but they are unavoidable!

Richard P. Feynman foresaw the necessity to include quantum physics in simulations in 1981 [37]

**“I’m not happy with all the analyses that go with just the classical theory, because nature isn’t classical, dammit, and if you want to make a simulation of nature, you’d better make it quantum mechanical, and by golly it’s a wonderful problem, because it doesn’t look so easy.”**

Sterile neutrino detection depends upon the particle physics model. There are sterile neutrino models where the keV sterile is stable and thus hard to detect (see for example [20]).

Detection may proceed through astronomical observations of X-ray keV sterile decay from galaxy halos and by direct detection of steriles in laboratory experiments.

Mare [24], Katrin [25], ECHo [26] and Project 8 [27] are expected to provide bounds on the mixing angles. However, for a particle detection, a dedicated beta decay experiment and/or electron capture experiment seem necessary to find sterile neutrinos with mass around 2 keV. In this respect, calorimetric techniques seem well suited.

The best nuclei for study are:  $^{187}\text{Re}$  and Tritium for beta decay and  $^{163}\text{Ho}$  for electron capture

The search of DM particles with mass around 2 keV is a promisory avenue for future trascendental discoveries.

- 
- [1] D. Boyanovsky, H J de Vega, N. G. Sanchez, Phys. Rev. **D 78**, 063546 (2008).  
 [2] H. J. de Vega, N. G. Sánchez, Phys. Rev. **D85**, 043516 (2012) and **D85**, 043517 (2012).  
 [3] C. Destri, H. J. de Vega, N. G. Sanchez, arXiv:1204.3090, New Astronomy **22**, 39 (2013) and arXiv:1301.1864.  
 [4] G. Gilmore et al., Ap J, 663, 948 (2007).  
 [5] M. Walker, J. Peñarrubia, Ap. J. 742, 20 (2011).  
 [6] P. Salucci et al., MNRAS, 378, 41 (2007).  
 [7] H. J. de Vega, P. Salucci, N. G. Sanchez, New Astronomy **17**, 653 (2012) and references therein.

- [8] J. D. Simon, M. Geha, *Ap J*, 670, 313 (2007) and references therein.
- [9] J. P. Brodie et al., *AJ*, 142, 199 (2011). B. Willman and J. Strader, *AJ*, 144, 76 (2012). J. D. Simon et al., *Ap. J.* 733, 46 (2011) and references therein. J. Wolf et al., *MNRAS*, 406, 1220 (2010) and references therein. G. D. Martinez et al., *Ap J*, 738, 55 (2011).
- [10] H. J. de Vega, N. G. Sánchez, *Mon. Not. R. Astron. Soc.* **404**, 885 (2010) and *Int. J. Mod. Phys. A* **26**, 1057 (2011).
- [11] P. Colín, O. Valenzuela, V. Avila-Reese, *Ap J*, 542, 622 (2000). J. Sommer-Larsen, A. Dolgov, *Ap J*, 551, 608 (2001). L. Gao and T. Theuns, *Science*, 317, 1527 (2007).
- [12] M. R. Lovell et al., *MNRAS*, 420, 2318 (2012).
- [13] A. V. Tikhonov et al., *MNRAS*, 399, 1611 (2009).
- [14] E. Papastergis et al., *Ap J*, 739, 38 (2011), J. Zavala et al., *Ap J*, 700, 1779 (2009).
- [15] A. V. Macciò, S. Paduroiu, D. Anderhalden, A. Schneider, B. Moore, *MNRAS*, 424, 1105 (2012). S. Shao et al. arXiv:1209.5563, *MNRAS* in press.
- [16] Highlights and conclusions of the Chalonge Colloquiums and Workshops: arXiv:1203.3562, arXiv:1109.3187, arXiv:1009.3494, arXiv:1007.2411
- [17] N. Menci, F. Fiore, A. Lamastra, arXiv:1302.2000.
- [18] L. Danese, H. J. de Vega, A. Lapi, P. Salucci, N. Sanchez (in preparation).
- [19] H J de Vega, O. Moreno, E. Moya, M. Ramón Medrano, N. Sánchez, *Nucl. Phys.* **B866**, 177 (2013).
- [20] A. Merle, arXiv:1302.2625.
- [21] R N Mohapatra, P B Pal, ‘Massive neutrinos in physics and astrophysics’, World Scientific, Singapore, 2004.
- [22] M. Loewenstein, A. Kusenko, P. L. Biermann, *Astrophys.J.* 700 (2009) 426-435 M. Loewenstein, A. Kusenko, *Astrophys.J.* 714 (2010) 652 and 751 (2012) 82.
- [23] C. R. Watson et al. *JCAP*, 03, 018 (2012).
- [24] <http://mare.dfm.uninsubria.it/frontend/exec.php>
- [25] <http://www.katrin.kit.edu/>
- [26] L. Gastaldo, lecture at the 3rd. NuMass Workshop, Milano Bicocca, Italy, February 2013.
- [27] <http://www.npl.washington.edu/project8/>
- [28] <http://xenia.msfc.nasa.gov/>
- [29] A. Kogut et al., *JCAP* 07, 025 (2011).
- [30] G. Raffelt, S. Zhou, *PRD* 83, 093014 (2011).
- [31] G. Steigman, *Adv. in High Energy Phys.* 268321 (2012).
- [32] G. Steigman, arXiv:1303.0049.
- [33] P. A. R. Ade et al., Planck 2013 results. XVI. arXiv:1303.5076.
- [34] J. Kopp et al. arXiv:1303.3011 and references therein.
- [35] S. N. Gninenko, *Phys. Rev. D*85, 051702(R) (2012) and references therein.
- [36] M. Drewes, arXiv:1303.6912
- [37] R. P. Feynman, Lecture at the 1st. Conference on Physics and Computation, MIT 1981, *Int. J. Theor. Phys.* **21**,467(1982).